Inorg. Chem. **2007**, *46*, 4446–4457

New BEDT-TTF/$[Fe(C_5O_5)_3]^{3-}$ Hybrid System: Synthesis, Crystal Structure, and Physical Properties of a Chirality-Induced α Phase and a Novel Magnetic Molecular Metal

Eugenio Coronado,[†] Simona Curreli,[†] Carlos Giménez-Saiz,[†] Carlos J. Gómez-García,*[,†] Paola Deplano,[‡] Maria Laura Mercuri,*[,‡] Angela Serpe,[‡] Luca Pilia,[‡] Christophe Faulmann,[§] and Enric Canadell[||]

Instituto de Ciencia Molecular, Universidad de Valencia, Pol. La Coma, E-46980 Paterna, Spain, Dipartimento di Chimica Inorganica ed Analitica, S.S. 554-Bivio per Sestu-I09042 Monserrato (Cagliari), Italy, Equipe Molécules et Matériaux, LCC-CNRS, 205 route de Narbonne, 31077 Toulouse Cedex 04, France, and ICMAB (CSIC), Campus de la UAB, 08193 Bellaterra, Spain

Received November 13, 2006

The paramagnetic and chiral anion $[Fe(C_5O_5)_3]^{3-}$ ($C_5O_5^{2-}$ = croconate) has been combined with the organic donor BEDT-TTF (=ET = bis(ethylenedithio)tetrathiafulvalene) to synthesize a novel paramagnetic semiconductor with the first chirality-induced α phase, α-(BEDT-TTF)$_5$[Fe(C$_5$O$_5$)$_3$]·5H$_2$O (**1**), and one of the few known paramagnetic molecular metals, β-(BEDT-TTF)$_5$[Fe(C$_5$O$_5$)$_3$]·C$_6$H$_5$CN (**2**). Both compounds present layers of BEDT-TTF molecules, with the α or β packing modes, alternating with layers containing the high-spin $S = 5/2$ Fe(III) anions and solvent molecules. In the α phase, the alternation of the chiral $[Fe(C_5O_5)_3]^{3-}$ anions along the direction perpendicular to the BEDT-TTF chains induces an alternation of the tilt angle of the BEDT-TTF molecules, giving rise to the observed α phase. The α phase presents a semiconductor behavior with a high room-temperature conductivity (6 S·cm^{-1}) and an activation energy of 116 meV. The β phase presents a metallic behavior down to ca. 120 K, where a charge localization takes place with a reentrance to the metallic state below ca. 20 K followed by a metal–semiconductor transition at ca. 10 K. The magnetic properties are dominated by the paramagnetic $S = 5/2$ $[Fe(C_5O_5)_3]^{3-}$ anion with an extra Pauli-type paramagnetism in the metallic β phase. The ESR spectra confirm the presence of the high-spin Fe(III)-containing anion and show a progressive localization in the organic sublattice along with an antiferromagnetic coupling below ca. 120 K that, in the metallic β phase, could be at the origin of the transition from the metallic to the activated conductivity regime. The correlation between crystal structure and conductivity behavior has been studied by means of tight-binding band structure calculations which provide a rationalization of the charge distribution and conductivity results.

Introduction

One of the most active areas in molecular science in the past decade has been the search for multifunctionality in molecular materials, particularly the combination of magnetic with electrical properties.[1] One of the aims of this strategy is to investigate if metallic conductivity can stabilize indirect exchange interactions in the localized magnetic moments thanks to the conducting electrons (indirect exchange). To reach this goal, the most used strategy has been the synthesis of radical salts containing paramagnetic anionic metal complexes with different sizes and geometries[1] combined with organic donors of the tetrathiafulvalene (TTF) family since this family has provided most of the known examples of molecular metals and superconductors.[2] Although this strategy has led to the synthesis of a large number of radical salts containing paramagnetic anions, most of them are

* To whom correspondence should be addressed. E-mail: carlos.gomez@uv.es (C.J.G.-G.), mercuri@unica.it (M.L.M.). Fax: +34.963543273 (C.J.G.-G.).
[†] Universidad de Valencia.
[‡] Universitá di Cagliari.
[§] LCC-CNRS.
[||] ICMAB.

(1) (a) Coronado, E.; Day, P. *Chem. Rev.* **2004**, *104*, 5419. (b) Enoki, T.; Miyazaki, A. *Chem. Rev.* **2004**, *104*, 5449. (c) Kobayashi, H.; Cui, H. B.; Kobayashi, A. *Chem. Rev.* **2004**, *104*, 5265.

(2) Williams, J. M.; Ferraro, J. R.; Thorn, R. J.; Carlson, K. D.; Geiger, U.; Wang, H. H.; Kini, A. M.; Whangbo, M. H. *Organic Superconductors: Synthesis, Structure, Properties and Theory*; Grimes, R. N., Ed.; Prentice Hall: Englewood Cliffs, NJ, 1992.

10.1021/ic062152m CCC: $37.00
Published on Web 04/28/2007

semiconductors or insulators,[1] precluding the existence of any indirect exchange interaction between the paramagnetic centers mediated by the delocalized electrons. Only in a few cases a metallic conductivity has been observed in this paramagnetic salts,[1] and among these, the number of examples where a noticeable indirect exchange interaction has been observed is very small.[3] The radical salt (BET-TTF)$_2$[$FeCl_4$] (BET-TTF = bis(ethylenethio)tetrathiafulvalene), which presents a metallic conductivity from room temperature down to 20 K and displays a weak, although noticeable, antiferromagnetic coupling between the Fe(III) ions, is one of these rare examples.[3a]

Other important milestones in the area of conducting and magnetic molecular materials are (1) the synthesis of the family (per)$_2$M(mnt)$_2$ (M = Pt, Pd, Ni, and Fe; per = perylene, mnt = maleonitriledithiolate = $S_2C_2(CN)_2$),[4] the first examples of paramagnetic molecular metals, (2) the synthesis of (BEDT-TTF)$_3$[$CuCl_4$]·H_2O,[5] the first paramagnetic molecular metal in the TTF family, (3) the synthesis of (BEDT-TTF)$_4$[$(H_3O)Fe(C_2O_4)_3$]·PhCN ($C_2O_4^{2-}$ = oxalate dianion), the first molecular paramagnetic superconductor,[6] (4) the synthesis of (BEDT-TTF)$_3$[$MnCr(C_2O_4)_3$],[7] the first molecular metallic ferromagnet, (5) the synthesis of κ-$BETS_2$[$FeBr_4$] (BETS = bis(ethylenedithio)tetraselenafulvalene),[1c,8] the first antiferromagnetic superconductor, and (6) the synthesis of λ-$BETS_2$[$FeCl_4$], the first field-induced superconductor.[1c,9]

Among these results, the series of paramagnetic superconductors and metals prepared by Day et al. using the octahedral $[M(C_2O_4)_3]^{3-}$ complexes and formulated as (BEDT-TTF)$_4$[$A^IM^{III}(ox)_3$]·solvent (A^+ = H_3O, K, and NH_4; M^{III} = Cr, Fe, Co, Ga, and Al; solvent = C_6H_5CN, $C_6H_5NO_2$, C_5H_5N, and CH_2Cl_2) constitutes a very promising and versatile family.[1a] In this series, enlarged very recently with PhF, PhCl, and PhBr as solvents by some of us,[10] up to eight paramagnetic superconductors have been reported, with critical temperatures ranging from 1.1 to 7.5 K.[1a,6,10] Day and co-workers have clearly demonstrated that the transport properties are related to structural changes and/or small changes of the components of these salts.[1a,6] To date, changes have been made on the monovalent cation (A^+), on the metal ion (M^{III}), and on the solvent molecule. As a progression of these studies, it seems interesting to synthesize new BEDT-TTF salts with M(III) complexes having chelating ligands with coordination modes similar to those of oxalate. One of these ligands is the croconate dianion ($C_5O_5^{2-}$ = dianion of croconic acid = 4,5-dihydroxycyclopent-4-ene-1,2,3-trione), which is the $n = 5$ member of the cyclic oxocarbons of formula $C_nO_n^{2-}$ ($n = 3-6$ for deltate, squarate, croconate, and rhodizonate anions, respectively). This aromatic series, which is stabilized by electron delocalization of π-electrons over the ring, has received considerable attention from both theoretical and experimental points of view.[11] Moreover, theoretical calculations have shown the very low aromatic character of this dianion (Scheme 1).[12]

Scheme 1. Resonant Structures of the Croconate $(C_5O_5)^{2-}$ Ligand

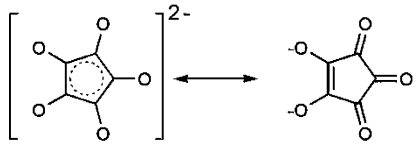

Both X-ray and solution studies have shown similarities between croconate and oxalate ligands supporting a chelating coordination mode.[13] The ligand properties and its coordination modes with first row transition divalent metals have been well described very recently by Julve et al.,[11] who have also shown the ability of croconate to mediate magnetic interactions (as observed in oxalate-bridged complexes).[14] Keeping in mind the analogies in the coordination chemistry of oxalate and croconate, we report in this work the synthesis, X-ray structure, and physical properties of two new radical salts obtained with the $[Fe(C_5O_5)_3]^{3-}$ anion and BEDT-TTF. These two salts, formulated as α-(BEDT-TTF)$_5$[$Fe(C_5O_5)_3$]·$5H_2O$ (**1**) and β-(BEDT-TTF)$_5$[$Fe(C_5O_5)_3$]·C_6H_5CN (**2**), present the same donor:anion stoichiometry and differ only in the packing motif of the BEDT-TTF molecules and in the solvent molecules. Salts **1** and **2** are the first examples of radical salts containing the chiral and paramagnetic $[Fe(C_5O_5)_3]^{3-}$ anion, whose synthesis, structural, and magnetic characteriza-

(3) (a) Coronado, E.; Falvello, L. R.; Galán-Mascarós, J. R.; Giménez-Saiz, C.; Gómez-García, C. J.; Lauhkin, V. N.; Pérez-Benítez, A.; Rovira, C.; Veciana, J. *Adv. Mater.* **1997**, *9*, 984. (b) Yamaguchi, K.; Kitagawa, Y.; Onishi, T.; Isobe, H.; Kawakami, T.; Nagao. H.; Takamizawa, S. *Coord. Chem. Rev.* **2002**, *226*, 235 and references therein.

(4) (a) Alcácer, L.; Novais, H.; Pedroso, F.; Flandrois, S.; Coulon, C.; Chasseau, D.; Gaultier, J. *Solid State Commun.* **1980**, *35*, 945. (b) Gama, V.; Henriques, R. T.; Almeida, M.; Alcácer, L. *Synth. Met.* **1991**, *42*, 2553. (c) Almeida, M.; Henriques, R. T. In *Handbook of Organic Conductive Molecules and Polymers, Vol. 1, Charge Transfer Salts, Fullerenes and Photoconductors*; Nalva, H. S., Ed.; John Willey & Sons Ltd.: New York, 1997.

(5) (a) Gudenko, A. V.; Ginodman, V. B.; Korotkov, V. E.; Koshelap, A. V.; Kushch, N. D.; Laukhin, V. N.; Rozenberg, L. P.; Khomenko, A. G.; Shibaeva, R. P.; Yagubskii, E. B. In *The Physics and Chemistry of Organic Superconductors*; Saito, G., Kagoshima, G., Eds.; Springer-Verlag: Berlin, 1990. (b) Kurmoo, M.; Mallah, T.; Marsden, L.; Allan, M.; Friend, R. H.; Pratt, F. L.; Hayes, W.; Chasseau, D.; Bravic, G.; Ducasse, L.; Day, P. *J. Am Chem. Soc.* **1992**, *114*, 10722.

(6) (a) Kurmoo, M.; Graham, A. W.; Day, P.; Coles, S. J.; Hursthouse, M. B.; Caulfield, J. L.; Singleton, J.; Pratt, F. L.; Hayes, W.; Ducasse, L.; Guionneau, P. *J. Am. Chem. Soc.* **1995**, *117*, 12209. (b) Martin, L.; Turner, S. S.; Day, P.; Mabbs, F. E.; McInnes, E. J. L. *J. Chem. Soc. Chem. Commun.* **1997**, 1367. (c) Rashid, S.; Turner, S. S.; Day, P.; Howard, J. A. K.; Guionneau, P.; McInnes, E. J. L.; Mabbs, F. E.; Clark, R. J. H.; Firth, S.; Biggs, T. *J. Mater. Chem.* **2001**, *11*, 2095.

(7) Coronado, E.; Galán-Mascarós, J. R.; Gómez-García, C. J.; Laukhin, V. N. *Nature* **2000**, *408*, 447.

(8) Fujiwara, H.; Fujiwara, E.; Nakazawa, Y.; Narymbetov, B. Zh.; Kato, K.; Kobayashi, H.; Kobayashi, A.; Tokumoto, M.; Cassoux, P. *J. Am. Chem. Soc.* **2001**, *123*, 306.

(9) Uji, S.; Shinagawa, H.; Terashima, T.; Yakabe, T.; Terai, Y.; Tokumoto, M.; Kobayashi, A.; Tanaka, H.; Kobayashi, H. *Nature* **2001**, *410*, 908.

(10) (a) Coronado, E.; Curreli, S.; Giménez-Saiz, C.; Gómez-García, C. J. *J. Mater. Chem.* **2005**, *15*, 1429. (b) Coronado, E.; Curreli, S.; Giménez-Saiz, C.; Gómez-García, C. J. *Synth. Met.* **2005**, *154*, 245.

(11) Calatayud, M. L.; Sletten, J.; Julve, M.; Castro, I. *J. Mol. Struct.* **2005**, *741*, 121 and references therein.

(12) Schleyer, P. R.; Najafian, K.; Kiran, B.; Jiao, H. *J. Org. Chem.* **2000**, *65*, 426.

(13) (a) Castro, I.; Faus, J.; Julve, M.; Journaux, Y.; Sletten, J. *J. Chem. Soc., Dalton Trans.* **1991**, 2533. (b) Castro, I.; Faus, J.; Julve, M.; Mollar, M.; Monge, A.; Gutiérrez-Puebla, E. *Inorg. Chim. Acta.* **1989**, *161*, 97.

(14) Castro, I.; Calatayud, M. L.; Lloret, F.; Sletten, J.; Julve, M. *J. Chem. Soc., Dalton Trans.* **2002**, 2397.

tion have been very recently described.[15] The structures and a preliminary characterization of these two salts have been recently published.[16]

Experimental Section

Synthesis. Black needlelike crystals of β-(BEDT-TTF)$_5$[Fe(C_5O_5)$_3$]·C_6H_5CN (**1**) were grown by using the previously described electrocrystallization technique.[17] BEDT-TTF (11.34 mg) was dissolved in 8 mL of benzonitrile, and the solution was placed in the anodic chamber of the cell. (Bu_4N)$_3$[Fe(C_5O_5)$_3$] (240.0 mg, donor:anion molar ratio 3:1) was dissolved in 16 mL of benzonitrile, and this solution was divided into the anodic and cathodic compartments. A current density of 1 μA·cm^{-2} (increased to 2 μA·cm^{-2} after 20 days) was applied. The single crystals were grown at 25 °C on a platinum wire electrode for a period of 60 days. Crystals of α-(BEDT-TTF)$_5$[Fe(C_5O_5)$_3$]·$5H_2O$ (**2**) were grown by using the same electrocrystallization technique and very similar conditions: BEDT-TTF (10.70 mg) was placed in the anode chamber of the electrocrystallization cell. (NBu_4)$_3$[Fe(C_5O_5)$_3$] (120.0 mg, donor:anion molar ratio 1.5:1) was dissolved in 20 mL of benzonitrile, and this solution was divided into the anodic and cathodic compartments. Black prismatic crystals were grown at 25 °C on a platinum wire electrode by applying a current density of 1 μA·cm^{-2} for a period of 36 days.

X-ray Crystallography. α-(BEDT-TTF)$_5$[Fe(C_5O_5)$_3$].5H_2O (1): $C_{65}H_{50}FeO_{20}S_{40}$, M_r = 2489.30, monoclinic, space group *C*2/c, a = 42.4125(5) Å, b = 11.2100(3) Å, c = 20.4336(3) Å, β = 114.8929(10)°, V = 8812.5(3) Å,^{3} Z = 4, T = 150(2) K, ρ_{calcd} = 1.876 g·cm^{-3}, μ(Mo Kα) = 11.89 cm^{-1}, collected reflections = 21 290, unique reflections = 10 937, Nonius Kappa CCD diffractometer (4.6° < 2θ < 56.6°), crystal size 0.20 × 0.10 × 0.05 mm^3. No absorption correction was performed. All non-hydrogen atoms were refined anisotropically. The positions of the H atoms on the C atoms were added into the calculated positions and refined with a riding model. The H atoms of the water molecules were not located. Final R ($I > 2\sigma(I)$): R_1 = 0.0466; wR_2 = 0.1104. Final R (all data): R_1 = 0.1036; wR_2 = 0.1327. Maximum/minimum residual electron density: 1.066/−0.584 e·Å^{-3}.

β-(BEDT-TTF)$_5$[Fe(C_5O_5)$_3$]·C_6H_5CN (2): $C_{72}H_{45}FeNO_{15}S_{40}$, M_r = 2502.34, triclinic space group $P\bar{1}$, a = 19.591(2) Å, b = 19.395(2) Å, c = 12.958 (1) Å, α = 103.19(1)°, β = 102.86(1)°, γ = 73.68(1)°, V = 4534.1(8) Å,^{3} Z = 2, T = 170 K, d_{calcd} = 1.833 g·cm^{-3}, μ(Mo Kα) = 11.534 cm^{-1}, collected reflections = 33 942, unique reflections = 12 379, Stoe IPDS diffractometer (4.4° < 2θ < 51.8°), crystal size 0.75 × 0.375 × 0.075 mm^3. Final R ($I > 2\sigma(I)$): R_1 = 0.0528; wR_2 = 0.0745. Final R (all data): R_1 = 0.1119; wR_2 = 0.2029. Maximum/minimum residual electron density: 0.467/−0.465 e·Å^{-3}.

The crystal structures of compounds **1** and **2** were determined from single-crystal X-ray diffraction data. Data were collected either with a Nonius Kappa CCD (for **1**) or a Stoe IPDS (for **2**) diffractometer using a graphite-monochromated Mo Kα radiation source (λ = 0.710 73 Å). The structures were solved by direct methods using the SIR97[18] program with the WinGX[19] graphical user interface, and the refinements were carried out with SHELX-97.[20] No absorption correction was applied for **1** while an empirical absorption correction (DIFABS) was performed for **2**. All non-hydrogen atoms were refined anisotropically. Hydrogen atoms on carbon atoms were included at calculated positions and refined with a riding model. Hydrogen atoms of water molecules were not located. Crystal data are tabulated in Table 1. CCDC 294531 and 269569 contain the supplementary crystallographic data for these salts. These data can be obtained free of charge from the Cambridge Crystallographic Data Centre via www.ccdc.cam.ac.uk/data_request/cif.

Table 1. X-ray Crystallographic Data for α-(BEDT-TTF)$_5$[Fe(C_5O_5)$_3$]·$5H_2O$ (**1**) and β-(BEDT-TTF)$_5$[Fe(C_5O_5)$_3$]·C_6H_5CN (**2**)

param	**1**	**2**
chem formula	$C_{65}H_{50}FeO_{20}S_{40}$	$C_{72}H_{45}FeNO_{15}S_{40}$
a (Å)	42.4125(5)	19.591(2)
b (Å)	11.2100(3)	19.395(2)
c (Å)	20.4336(3)	12.9581(12)
α (deg)	90	103.194(11)
β (deg)	114.8929(10)	102.859(11)
γ (deg)	90	73.680(10)
V (Å^3)	8812.5(3)	4534.1(8)
T/K	150(2)	170(2)
Z	4	2
fw	2489.30	2502.34
cryst syst	monoclinic	triclinic
space group	*C*2/*c*	$P\bar{1}$
ρ_{calcd}/g cm^{-3}	1.876	1.833
μ/mm^{-1}	1.189	1.153
$R(F_o)$, $R_w(F_o^2)$ [$I < 2\sigma(I)$]	0.0466, 0.1104	0.0528, 0.0745

Physical Properties. Variable-temperature susceptibility measurements were carried out in the temperature range 2−300 K with an applied magnetic field of 1 T on polycrystalline samples of 4.967 and 4.390 mg, for **1** and **2**, respectively, with a Quantum Design MPMS-XL-5 SQUID magnetometer. The susceptibility data were corrected for the sample holder (sealed plastic bags of ca. 5.0 mg), previously measured using the same conditions, and for the diamagnetic contributions of the salt as deduced by using Pascal's constant tables (χ_{dia} = −1275 × 10^{-6} and −1286.4 × 10^{-6} emu·K·mol^{-1} for **1** and **2**, respectively). Dc conductivity measurements over the range 2−300 K were performed with the four contacts method in 2 (for **1**) and 10 (for **2**) different single crystals, giving reproducible results in all the samples. Contacts between the crystals and platinum wires (25 μm diameter) were made using graphite paste. The samples were measured in a Quantum Design PPMS-9 with dc currents in the range 0.005−10 μA. The cooling and warming rates were 1 K/min, and the results were, within experimental error, identical in the cooling and warming sweeps and intensity independent (except for the transition from activated to metallic conductivity at low temperatures observed in **2**). ESR spectra were recorded in both X and Q bands with a Bruker E-500 ELEXSYS spectrometer in the temperature range 4−300 K on polycrystalline samples of both compounds. The X-band spectra were identical with those obtained in Q-band (although with a lower resolution), and therefore, only the Q-band ESR spectra are shown and discussed.

(15) Curreli, S.; Deplano, P.; Faulmann, C.; Mercuri, M. L.; Pilia, L.; Serpe, A.; Coronado, E.; Gómez-García, C. J. *Inorg. Chim. Acta* **2006**, *359*, 1177.
(16) Gómez-García, C. J.; Coronado, E.; Curreli, S.; Giménez-Saiz, C.; Deplano, P.; Mercuri, M. L.; Pilia, L.; Serpe, A.; Faulmann, C.; Canadell, E. *Chem. Commun.* **2006**, DOI: 10.1039/b610408h.
(17) (a) Emge, T. J.; Wang, H. H.; Beno, M. A.; Williams, J. M.; Whangbo, M. H.; Evain, M. *J. Am. Chem. Soc.* **1986**, *108*, 8215. (b) Stephens, D. A.; Rehan, A. E.; Compton, S. J.; Barkhau, R. A.; Williams, J. M. *Inorg. Synth.* **1986**, *24*, 135.
(18) Altomare, A.; Burla, M. C.; Camalli, M.; Cascarano, G.; Giacovazzo, C.; Guagliardi, A.; Moliterni, A. G. G.; Polidori, G.; Spagna, R. *J. Appl. Crystallogr.* **1999**, *32*, 115.
(19) Farrugia, L. J. *J. Appl. Crystallogr.* **1997**, *32*, 837.
(20) Sheldrick, G. M. *SHELX-97*; University of Göttingen: Göttingen, Germany, 1997.

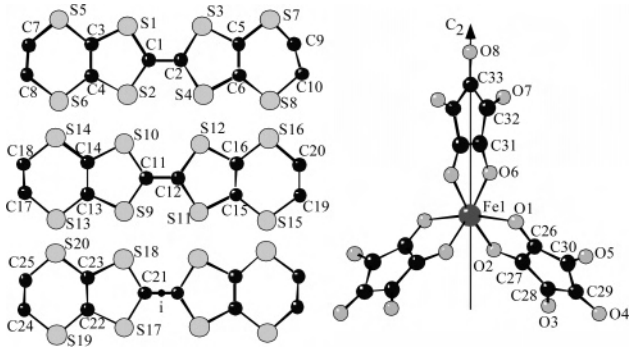

Figure 1. Labeling scheme for the three ET molecules and for the $[Fe(C_5O_5)_3]^{3-}$ anion in **1**.

Band Structure Calculations. The tight-binding band structure calculations were based upon the effective one-electron Hamiltonian of the extended Hückel method.[21] The off-diagonal matrix elements of the Hamiltonian were calculated according to the modified Wolfsberg−Helmholz formula.[22] All valence electrons were explicitly taken into account in the calculations, and the basis set consisted of double-ζ Slater-type orbitals for C and S and single-ζ Slater-type orbitals for H. The exponents, contraction coefficients, and atomic parameters for C, S, and H were taken from previous work.[23]

Results and Discussion

Synthesis. As described in the Experimental Section, both salts have been prepared under very similar conditions. The only changes are (i) the highest donor:anion ratio used in the synthesis of **1** (3:1 compared to 1.5:1 for **2**) and (ii) the longer crystallization period needed for **1** (60 days compared to 36 days for **2**). The synthesis of two different crystal phases has already been observed in other radical salts with TTF-type donors, although usually they present different stoichiometries and are prepared in quite different conditions. The presence of water molecules in the structure of **1**, also observed in other radical salts, seems to come from the trace water content of the benzonitrile solvent used in the synthesis.

Crystal Structure. α-(BEDT-TTF)$_5$[Fe(C$_5$O$_5$)$_3$]·5H$_2$O (1). The asymmetric unit of **1** contains 0.5 $[Fe(C_5O_5)_3]^{3-}$ unit, 2.5 BEDT-TTF molecules (ET1, ET2, and ET3, respectively), and 2.5 water molecules, giving rise to a 5:1 donor:anion stoichiometry. The $[Fe(C_5O_5)_3]^{3-}$ anion appears in a special position with the Fe atom and C33 and O8 atoms of one croconate ligand located on special positions (1/2, *y*, 1/4), corresponding to a C_2 axis. Figure 1 shows the labeling scheme for each BEDT-TTF molecule and for the anion.

The structure of **1** consists of alternating layers of BEDT-TTF molecules separated by layers of $[Fe(C_5O_5)_3]^{3-}$ anions and solvent (water in this case) molecules (Figure 2a). The BEDT-TTF molecules form parallel stacks along the *c* direction, following the sequence ···1−2−3−2−1··· with the molecular planes tilted an angle of ca. 22° with respect to the chain direction (Table S1, Supporting Information). Consecutive chains are tilted in opposite senses, giving rise to the so-called α phase,[2] called θ_{20} by Mori et al.[24] (Figure 2b). Furthermore, the BEDT-TTF molecules do not show a regular stack in the columns but present a dislocation every five molecules (between two ET1 type molecules, Figure 2a), following the periodicity in the arrangement of the anions, giving rise to the only known θ_{51} phase in Mori's notation (where 5 represents the number of molecules along the stack and 1 stands for the number of dislocations within the repeating unit).[24]

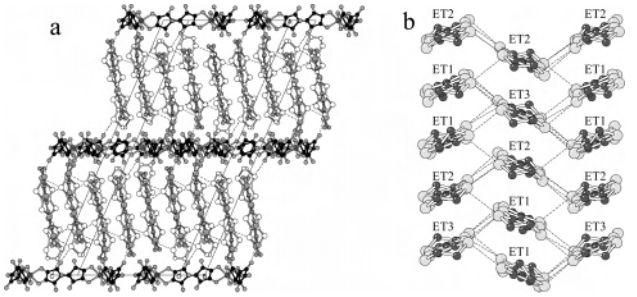

Figure 2. (a) View of the alternating cationic and anionic layers in **1** showing the two types of BEDT-TTF columns in each layer (in gray and white). (b) View of the BEDT-TTF layer showing the α packing. The intermolecular contacts shorter than the sum of the Van der Waals radii are indicated as dotted lines.

Table 2. Intrachain S···S Contacts Shorter than the Sum of the van der Waals Radii in β-(BEDT-TTF)$_5$[Fe(C$_5$O$_5$)$_3$]·C$_6$H$_5$CN (**2**)[a]

ET molecules	atoms	dist (Å)
ET1-ET2	S13−S23	3.423
ET1-ET2	S14−S24	3.572
ET1-ET2	S15−S25	3.514
ET1-ET2	S16−S26	3.532
ET4-ET5	S45−S53	3.595

[a] In salt α-(BEDT-TTF)$_5$[Fe(C$_5$O$_5$)$_3$]·5H$_2$O (**1**), there is no S···S contact shorter than the sum of the van der Waals radii.

As in many other α and θ phases, the interstack S···S distances are shorter than the intrastack ones. In fact, salt **1** presents many interchain distances, but no intrachain one, shorter than the sum of the Van der Waals radii (3.60 Å) (Tables 2 and 3). The three BEDT-TTF molecules are almost planar, and within a stack, the BEDT-TTF molecules are almost perfectly parallel to each other (their interplanar angles are smaller than 0.5°, Table S1). The distances between the average planes of each BEDT-TTF molecule in the chain are ET1-ET1 = 3.80(9) Å, ET1-ET2 = 3.64(6) Å, and ET2-ET3 = 3.67(7) Å (Table S1). It is noteworthy that the longest ET1−ET1 distance corresponds to the dislocation observed in the chain every five molecules. The interplanar angle between BEDT-TTF molecules of consecutive chains ranges between 44.0 and 45.3° (planes defined with the central "TTF" core, Table S1).

The terminal ethylene groups of the BEDT-TTF molecules adopt a twisted/boat conformation in ET1 and an eclipsed twisted conformations in ET2 and ET3 (Figure 2).

(21) Whangbo, M.-H.; Hoffmann, R. *J. Am. Chem. Soc.* **1978**, *100*, 6093.
(22) Ammeter, J.; Bürgi, H.-B.; Thibeault, J.; Hoffmann, R. *J. Am. Chem. Soc.* **1978**, *100*, 3686.
(23) Pénicaud, A.; Boubekeur, K.; Batail, P.; Canadell, E.; Auban-Senzier, P.; Jérome, D. *J. Am. Chem. Soc.* **1993**, *115*, 4101.
(24) Mori, T.; Mori, H.; Tanaka, S. *Bull. Chem. Soc. Jpn.* **1999,** *72*, 179.

Table 3. Interchain S···S Contacts Shorter than the Sum of the van der Waals Radii in α-(BEDT-TTF)$_5$[Fe(C$_5$O$_5$)$_3$]·5H$_2$O **(1)** and *β*-(BEDT-TTF)$_5$[Fe(C$_5$O$_5$)$_3$]·C$_6$H$_5$CN (**2**)

1				**2**			
atoms	dist (Å)	atoms	dist (Å)	atoms	dist (Å)	atoms	dist (Å)
S3−S14	3.430	S11−S14	3.523	S11−S11	3.371	S22−S43	3.448
S4−S19	3.528	S12−S13	3.494	S11−S13	3.449	S24−S31	3.383
S5−S17	3.534	S13−S16	3.532	S11−S52	3.404	S25−S56	3.586
S5−S19	3.423	S14−S19	3.399	S11−S54	3.597	S26−S47	3.508
S6−S11	3.504			S12−S51	3.492	S31−S35	3.577
S6−S18	3.485			S15−S58	3.365	S32−S38	3.572
S6−S20	3.436			S17−S58	3.470	S32−S48	3.501
S7−S20	3.489			S18−S47	3.389	S33−S33	3.493
S8−S19	3.339			S22−S41	3.538		

Table 4. Bond Lengths (Averaged Values) and Calculated Charges in the BEDT-TTF Molecules in α-(BEDT-TTF)$_5$[Fe(C$_5$O$_5$)$_3$]·5H$_2$O (**1**) and *β*-(BEDT-TTF)$_5$[Fe(C$_5$O$_5$)$_3$]·C$_6$H$_5$CN (**2**)

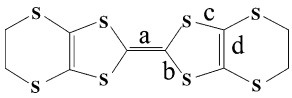

salt	ET molecule	*a* (Å)	*b* (Å)	*c* (Å)	*d* (Å)	δ^a	Q^b	Q_{total}
1	ET1 (×2)	1.361(4)	1.748(3)	1.763(3)	1.348(3)	0.8025	0.3(1)	3.3 ± 0.5
	ET2 (×2)	1.393(5)	1.728(3)	1.749(3)	1.359(3)	0.7255	0.9(1)	
	ET3 (×1)	1.387(6)	1.724(3)	1.748(3)	1.362(3)	0.7235	0.9(1)	
2	ET1 (×1)	1.399(16)	1.718(13)	1.725(13)	1.362(13)	0.68200	1.2(1)	3.4 ± 0.5
	ET2 (×1)	1.360(16)	1.729(13)	1.725(13)	1.360(13)	0.73375	0.9(1)	
	ET3 (×1)	1.316(15)	1.756(12)	1.754(12)	1.358(12)	0.83575	0.1(1)	
	ET4 (×1)	1.343(17)	1.733(14)	1.733(14)	1.382(14)	0.74125	0.8(1)	
	ET5 (×1)	1.349(14)	1.746(12)	1.746(12)	1.347(12)	0.79625	0.4(1)	

[a] $\delta = (b + c) - (a + d)$. [b] $Q = 6.347 - 7.463\delta$.

The central C═C bond distances in the three crystallographically independent BEDT-TTF molecules suggest that the charge is not homogeneously distributed over the three BEDT-TTF molecules (Table 4). Thus the analysis of the bond distances by using the method of Day et al.[25] shows that ET1, ET2, and ET3 bear charges of +0.3, +0.9, and +0.9, respectively (Table 4). These values are given with an accuracy of ca. ±0.1 and lead to a total charge of 3.3 ± 0.5, in good agreement with the value of +3 expected for this salt (note that in the formula unit there are two ET1 and ET2 molecules and one ET3 molecule).

The anionic layer in **1** is formed by isolated [Fe(C$_5$O$_5$)$_3$]$^{3-}$ units and water molecules (Figure 3) with a shortest interanion O···O distance (O4−O5) of 3.122 Å. The Fe(III) ion is surrounded by three croconate ligands acting as 1,2-bidentate with O−Fe−O angles of 82.23(10)° (O1−Fe−O2) and 82.17(15)° (O6−Fe−O6) (Table 5) and bite parameters of 1.315 and 1.314, respectively, close to those found in the two only known salts of this anions[15] and in oxalate complexes with a similar 1,2-bidentate coordination.[6,10,26] The Fe−O distances (2.038, 2.040, and 2.046 Å) (Table 5) are also very similar to those found in **2** and in the Fe(III) tris-(oxalate) complex.[6,10,26]

The [Fe(C$_5$O$_5$)$_3$]$^{3-}$ anions form zigzag rows, separated by water molecules, along the c direction with Δ enantiomers alternating with the Λ ones, giving rise to an achiral structure (Figure 3). Since the orientation of the planes of the croconate ligands are different for each enantiomer (Figure 4), this alternation of the chirality of the [Fe(C$_5$O$_5$)$_3$]$^{3-}$ anions along the *b*-axis (perpendicular to the BEDT-TTF chains) induces in salt **1** a similar alternation in the tilt angles of the BEDT-TTF molecules. Thus, each Δ enantiomer induces a "right-turned" column of BEDT-TTF molecules in the organic layer above and a "left-turned" column in the layer below. Of

Table 5. Selected Bond Lengths (Å) and Angles (deg) in the [Fe(C$_5$O$_5$)$_3$]$^{3-}$ Anion in α-(BEDT-TTF)$_5$[Fe(C$_5$O$_5$)$_3$]·5H$_2$O (**1**) and *β*-(BEDT-TTF)$_5$[Fe(C$_5$O$_5$)$_3$]·C$_6$H$_5$CN (**2**)

1		**2**	
atoms	dist (Å)	atoms	dist (Å)
Fe1−O6	2.038(3)	Fe1−O111	2.001(8)
Fe1−O1	2.040(2)	Fe1−O110	2.014(7)
Fe1−O2	2.046(3)	Fe1−O101	2.022(8)
		Fe1−O105	2.025(9)
		Fe1−O115	2.056(8)
		Fe1−O106	2.057(9)

1		**2**	
atoms	angle (deg)	atoms	angle (deg)
O6−Fe1−O6	82.17(15)	O111−Fe1−O110	93.0(3)
O6−Fe1−O1	95.13(10)	O111−Fe1−O101	167.1(3)
O6−Fe1−O1	94.81(10)	O110−Fe1−O101	98.6(3)
O1−Fe1−O1	166.80(16)	O111−Fe1−O105	91.9(4)
O6−Fe1−O2	172.23(11)	O110−Fe1−O105	88.2(3)
O6−Fe1−O2	90.75(10)	O101−Fe1−O105	82.8(4)
O1−Fe1−O2	82.23(10)	O111−Fe1−O115	83.1(3)
O1−Fe1−O2	88.98(10)	O110−Fe1−O115	175.9(4)
O2−Fe1−O2	96.49(15)	O101−Fe1−O115	85.4(3)
		O105−Fe1−O115	93.5(3)
		O111−Fe1−O106	98.9(4)
		O110−Fe1−O106	82.1(3)
		O101−Fe1−O106	88.4(3)
		O105−Fe1−O106	165.8(3)
		O115−Fe1−O106	96.9(3)

(25) Guionneau, P.; Kepert, C. J.; Bravic, G.; Chasseau, D.; Truter, M. R.; Kurmoo, M.; Day, P. *Synt. Met.* **1997**, *86*, 1973.
(26) Merrachi, H.; Mentzen, B. F.; Chassagneux, F.; Bouix, J. *Rev. Chim. Miner.* **1987**, *24*, 56.

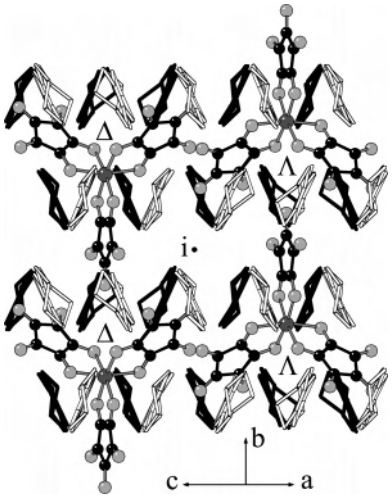

Figure 3. View of the anionic layer of **1** showing the zigzag rows of anions with alternating chirality and the organic layers above (white) and below (black) the anionic layer. The point indicates the location of the inversion center in the anionic layer.

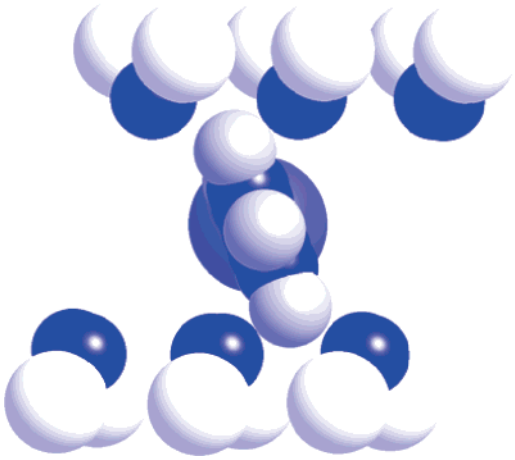

Figure 4. View of the croconate ligand located over the BEDT-TTF chains and the different orientation of the BEDT-TTF chains induced above and below it. For clarity, only the terminal $-S-CH_2-CH_2-S-$ groups of the BEDT-TTF molecules are shown.

course, the Λ enantiomer induces the opposite packing scheme. This effect is possible thanks to the presence of a supramolecular interlayer interaction, together with the steric effects, as clearly evidenced in the interaction between the BEDT-TTF molecules and the croconate ligand pointing toward the interlayer space (Figure 4). In fact, salt **1** shows one very short S···O cation−anion interaction, S15−O5 = 3.01 Å, much shorter than the sum of the corresponding Van der Waals radii (3.32 Å). Therefore, the alternation of Δ and Λ enantiomers along the *b*-axis is the driving force that induces the same alternation of "right" and "left" turned columns along this direction, giving rise to the α-packing observed in the organic sublattice in salt **1**. We can also see that the disposition of the anions implies that the inversion center of the organic layer is located in the interchain space (Figure 3), giving rise to the observed alternation of the tilt angle along the c-axis. As far as we know, only the salt $(BEDT\text{-}TTF)_9[H_4Co_2Mo_{10}O_{38}]$ shows a similar alternation in the donor stacks induced by the chirality of the anion,[27] although in this salt the huge size of the chiral

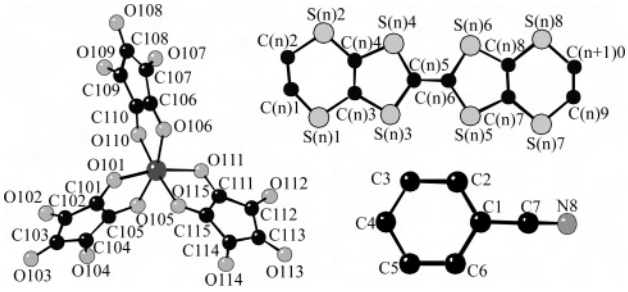

Figure 5. Labeling scheme for each ET(*n*) molecule ($n = 1-5$), for the solvent molecules, and for the $[Fe(C_5O_5)_3]^{3-}$ anion in **2**.

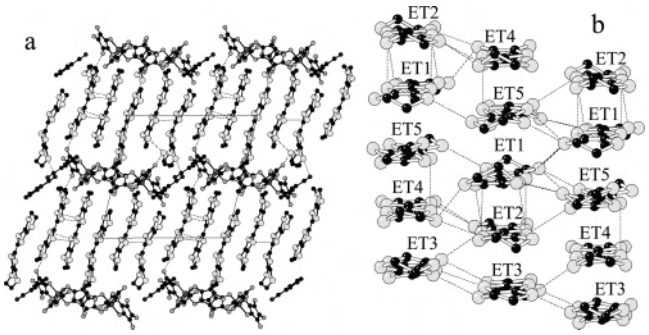

Figure 6. (a) View of the alternating cationic and anionic layers in **2**. (b) View of the BEDT-TTF layer showing the β packing. The intermolecular contacts shorter than the sum of the Van der Waals radii are indicated as dotted lines.

anion induces an alternation of the BEDT-TTF stacks with a periodicity of three stacks, giving rise to a θ_{33} phase in Mori's notation.[24]

β-(BEDT-TTF)$_5$[Fe(C$_5$O$_5$)$_3$]·C$_6$H$_5$CN (2). The asymmetric unit of **2** contains one $[Fe(C_5O_5)_3]^{3-}$ unit, one benzonitrile molecule, and five independent BEDT-TTF molecules, all in general positions, giving rise, as in **1**, to a 5:1 donor:anion stoichiometry. Figure 5 shows the labeling scheme for each ET(*n*) molecule ($n = 1-5$), for the solvent molecules, and for the anion.

The structure of **2** also consists of alternating layers of BEDT-TTF molecules separated by layers of $[Fe(C_5O_5)_3]^{3-}$ anions and solvent molecules (Figure 6a). The BEDT-TTF molecules form parallel stacks along the *a* direction, following the sequence ···1−2−3−4−5··· with the molecular planes orthogonal to the chain direction, giving rise to the so-called β phase (Figure 6b).[2,28] As in many other β phases, the interstack S···S distances are shorter than the intrastack ones. Thus, many intra- and interchain distances shorter than the sum of the Van der Waals radii (3.60 Å) can be observed (Tables 2 and 3) rendering a true two-dimensional character to this salt. The interplanar distances within the chain show that the five BEDT-TTF molecules are grouped into a trimer (ET1−ET2−ET3) and a dimer (ET4−ET5). The distances between the average planes of each BEDT-TTF molecule in the trimer are very similar (ET1−ET2 = 3.45(5) Å and ET2−ET3 = 3.52(4) Å) and slightly longer than the intradimer one, ET4-ET5 = 3.28(15) Å. The dimer−trimer

(27) (a) Coronado, E.; Giménez-Saiz, C.; Gómez-García, C. J. *Coord. Chem. Rev.* **2005**, *249*, 1776. (b) Coronado, E.; Curreli, S.; Giménez-Saiz, C.; Gómez-García, C. J.; Roth, J. *Synth. Met.* **2005**, *154*, 241.
(28) Mori, T. *Bull. Chem. Soc. Jpn.* **1998**, *71*, 2509.

distances are much longer (ET3−ET4 = 4.01(10) Å and ET1−ET5 = 4.34(6) Å) (Figure 6, Table S1). Note that the unusually long (or short) interplanar distances observed between ET3−ET4 and ET1−ET5 (or ET4 and ET5) arises from the strong distortion from planarity observed in ET3 and ET5. Within a stack, the BEDT-TTF molecules are not perfectly parallel to each other although their interplanar angles are very small: they vary from 0.24 to 4.40° (planes defined with the central "TTF" core $S_2C{=}CS_2$, Table S1). The intramolecular bond lengths within ET3 and ET5 also reflect their distortion compared to the other BEDT-TTF molecules (Table 4). The strong deviations from planarity of ET5 might be explained from the numerous contacts that occur among ET5, the anion, and the solvent molecule. In fact, ET5 is the only BEDT-TTF molecule to exhibit a short S···N contact (S57−N8 = 3.21(2) Å) with the solvent C_6H_5CN molecule. The terminal ethylene groups of the BEDT-TTF molecules adopt a twisted/boat conformation in ET1 and ET5, an eclipsed twisted conformation in ET2 and ET3, and a staggered boat conformation in ET4 (Figure 6).

The large differences between the intramolecular distances within each BEDT-TTF molecule strongly suggest that the positive charge carried by each BEDT-TTF molecule is not equivalent. The central C=C bond length of 1.316 Å in ET3 is indicative of a neutral BEDT-TTF molecule, whereas a value of 1.399 Å in ET1 and 1.360 Å in ET2 suggest that the dimer ET1−ET2 is more positively charged than the dimer ET4−ET5, where these bond lengths are 1.343 and 1.349 Å (Table 4). Indeed, with the same method as in **1**, it is found that ET1, ET2, ET3, ET4, and ET5 carry charges of +1.2, +0.9, +0.1, +0.8, and +0.4, respectively. These values are given with an accuracy of ca. ±0.1 leading to a total charge of 3.4 ± 0.5, in agreement with the value of +3 expected for the organic sublattice in this salt (Table 4) (note that in salt **2** there is one ET molecule of each type per anion).

The anionic layer is also formed by isolated $[Fe(C_5O_5)_3]^{3-}$ units and C_6H_5CN solvent molecules (Figure 7). Due to a different packing motif in the anionic layer, the shortest interanion O···O distance in salt **2** (O102−O104 = 3.377 Å) is slightly longer than in salt **1** (3.122 Å). The Fe(III) ion is also surrounded by three croconate ligands acting as 1,2-bidentate with O−Fe−O angles of 82.8(4)° (O101−Fe−O105), 83.1(3)° (O111−Fe−O115), and 82.1(3)° (O106−Fe−O110) (Table 5) and bite parameters of 1.323, 1.337, and 1.314, respectively, close to those found in the same anion in **1** and in other oxalate complexes. The Fe−O distances (2.001−2.057 Å) (Table 5) are very similar to those found in salt **1** (2.038−2.046 Å), in the two other known salts of this anion,[15] and in the Fe(III) tris(oxalate) complex.[6,10,26] The $[Fe(C_5O_5)_3]^{3-}$ anions form double rows along the *c* direction containing a single row of Δ enantiomers and a single row of Λ enantiomers, rendering this compound achiral since there is the same number of Δ and Λ enantiomers in the structure. These double rows are separated by rows of C_6H_5CN solvent molecules (Figure 7). Despite the chirality of the $[Fe(C_5O_5)_3]^{3-}$ anion, there is no

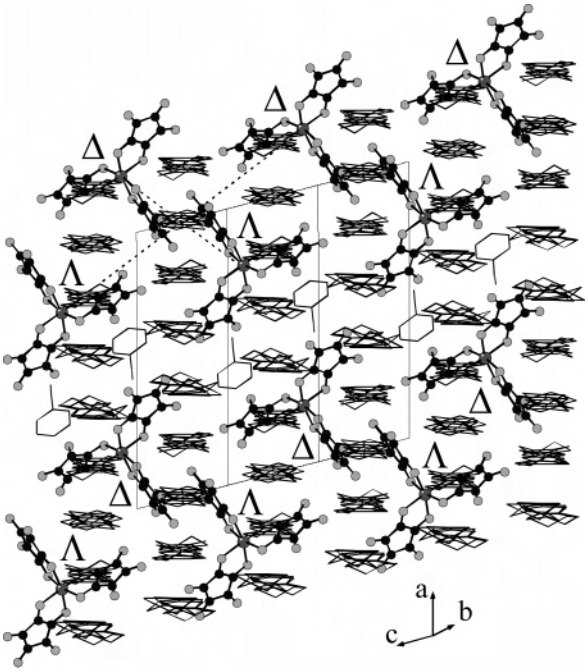

Figure 7. View of the anionic and cationic layers of **2** showing the *β*-type packing and the double rows of anions along the *c* direction, with different chirality. The crossing point of the dotted lines indicates the location of the inversion center in the anionic layer.

influence in the packing of the organic layer (contrary to salt **1**) because now the alternation along the c direction (perpendicular to the chain direction) is different. Thus, in salt **2**, both enantiomers are located in equivalent positions from the organic layer point of view since the iron atom lay over the interchain space and the inversion center in the inorganic layer is located over the BEDT-TTF chain (Figure 7).

Besides the above-mentioned short distance between one BEDT-TTF molecule (ET5) and the N atom of the C_6H_5CN solvent molecule, there are up to five S···O cation−anion interactions in the range 2.887−3.208 Å, shorter than the sum of the van der Waals radii (3.32 Å).

Electrical Properties. α-(BEDT-TTF)$_5$[Fe(C$_5$O$_5$)$_3$]·5H$_2$O (1). Although the room-temperature conductivity of this salt (ca. 6 S·cm^{-1}) is quite high (and similar to that of **2**; see below), the thermal variation of the resistivity shows a continuous decrease with decreasing the temperature and shows a classical semiconducting regime with an activation energy of 116 meV (inset in Figure 8).

***β*-(BEDT-TTF)$_5$[Fe(C$_5$O$_5$)$_3$]·C$_6$H$_5$CN (2).** The thermal variation of the dc electrical resistivity of up to 10 different single crystals of the *β* phase shows in all cases very similar behaviors with very high conductivities at room temperature, in the range 5−50 S·cm^{-1}. The resistivity values in all cases fall with decreasing temperature, reaching minima at ca. 120 K. At lower temperatures the resistivity rises to a maximum at ca. 20 K and then it falls again before exhibiting a second minimum at ca. 4−10 K, depending on the intensity of the dc current (Figure 8). Below this temperature the resistivity increases in a classical semiconducting regime although with a very low activation energy (0.2−0.5 meV). This behavior indicates that the title compound is metallic down to ca. 120

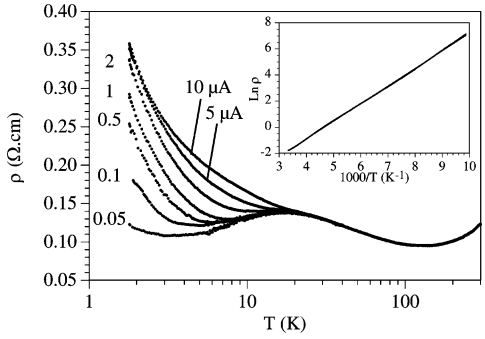

Figure 8. Thermal variation of the dc resistivity at different current intensities (in μA) for **2**. Inset: Arrhenius plot of the thermal variation of the resistivity of **1**.

K. Below this temperature the conductivity becomes thermally activated although it does not follow an Arrhenius law ($\ln \sigma \propto T^{-1}$) nor a hopping regime where $\ln \sigma \propto T^{-\alpha}$ (with $\alpha = 1/3$ or $1/4$). In fact, the Arrhenius plot ($\ln \rho$ vs $1/T$) shows a continuous change in the slope in the temperature range 120−20 K, excluding the idea of a classical semiconducting regime. A possible reason for this distinct behavior is the presence of a progressive charge localization, taking place below ca. 120 K, as also suggested by the ESR spectra (see below). Furthermore, the reentrance to the metallic state observed in the title compound below ca. 20 K supports the idea that the minimum in the resistivity at ca. 120 K is not a true metal−semiconductor transition. The current dependence of this reentrance also supports this idea. Thus, the maximum in the resistivity plot observed at ca. 20 K is progressively suppressed with increasing the current intensity and even disappears for dc current intensities above 5 μA (Figure 8). This kind of behavior, although unusual, has already been observed in other related BEDT-TTF salts with the chiral anions $[M(C_2O_4)_3]^{3-}$ (M^{III} = Ga, Fe, and Cr).[1,6]

Magnetic Properties. α-(BEDT-TTF)$_5$[Fe(C$_5$O$_5$)$_3$]·5H$_2$O (1). The thermal variation of the $\chi_m T$ product of the α phase shows a room-temperature value of ca. 4.5 emu·K·mol^{-1} that remains constant when the temperature is decreased to ca. 15 K. Below this temperature the $\chi_m T$ product sharply decreases to reach a value of ca. 3.6 emu·K·mol^{-1} at 2 K. This behavior is similar to that of salt **2** except for the linear decrease observed in the $\chi_m T$ product when decreasing the temperature and suggests that salt **1** essentially behaves as an $S = 5/2$ paramagnet. The decrease at low temperatures can be attributed to the presence of weak antiferromagnetic interactions between the Fe(III) ions and/or to the presence of a zero field splitting (ZFS) of the $S = 5/2$ Fe(III) ions. Thus, we have used two models to fit the magnetic data of **1**. (1) This first is a model of isolated $S = 5/2$ ions with ZFS (the Hamiltonian is written as $H = S\cdot D\cdot S$):[29] $\chi_m = (\chi_{||} + 2\chi_\perp)/3$ with

$$\chi_{||} = \frac{Ng^2\mu_B{}^2}{kT}\frac{1 + 9e^{-2x} + 25e^{-6x}}{4(1 + e^{-2x} + e^{-6x})}$$

and

$$\chi_\perp = \frac{Ng^2\mu_B{}^2}{kT}\frac{9 + (8/x)(1 - e^{-2x}) + (5/2x)(e^{-2x} - e^{-6x})}{4(1 + e^{-2x} + e^{-6x})}$$

and $x = |D|/kT$.

(2) The second is a simple Curie−Weiss law: $\chi_m = C/(T - \Theta)$. Both models show good agreements in the whole temperature region with the following sets of parameters: (1) C = 4.515(1) emu·K·mol^{-1}, corresponding to g = 2.0317(4) and $|D|$ = 3.10(3) K = 2.15(2) cm^{-1} (solid line in Figure 9); (2) C = 4.541(1) emu·K·mol^{-1}, corresponding to g = 2.0377(4) and Θ = −0.44(1) K = 0.30(1) cm^{-1} (dashed line in Figure 9). Note that the sign of D cannot be determined from powder measurements and that the D value may also include the weak antiferromagnetic coupling between the Fe(III) ions. Since both models give very good results, it is difficult to determine which one gives a better agreement, and therefore, we can conclude that most probably both effects are present in **1**. In fact, the ESR results show the presence of a ZFS in the Fe(III) ion of 0.94 cm^{-1}, indicating that in compound **1** both effects, a ZFS and an a weak antiferromagnetic coupling, are present, both of similar intensities (see below).

β-(BEDT-TTF)$_5$[Fe(C$_5$O$_5$)$_3$]·C$_6$H$_5$CN (**2**). The thermal variation of the molar magnetic susceptibility times the temperature ($\chi_m T$) of the β phase shows at room temperature a value of ca. 5.2 emu·K·mol^{-1} that decreases smoothly and linearly when lowering the temperature to reach a value of ca. 4.4 emu·K·mol^{-1} at ca. 15 K (Figure 9). This behavior indicates that **2** is, as salt **1**, essentially an $S = 5/2$ paramagnet but with an extra temperature-independent paramagnetic contribution (Pauli-type paramagnetism, typical of metallic salts). As in **1**, below ca. 15 K the $\chi_m T$ product of salt **2** shows a more rapid decrease due to the presence of a ZFS in the $S = 5/2$ Fe(III) ions and/or to weak antiferromagnetic interactions between the Fe(III) ions. As in **1**, we have fitted the magnetic data to two different models, although now we have added a temperature-independent paramagnetism ($N\alpha$) to account for the Pauli-type paramagnetism: (1) an isolated $S = 5/2$ ion with a ZFS[29] and an extra temperature-independent contribution ($N\alpha$), $\chi_m = (\chi_{||} + 2\chi_\perp)/3 + N\alpha$, and (2) a simple Curie−Weiss model also with an extra temperature-independent contribution ($N\alpha$), $\chi_m = C/(T - \Theta) + N\alpha$. Both models reproduce very satisfactorily the magnetic data of **2** in the whole temperature range with the following sets of parameters: (1) C = 4.665(4) emu·K·mol^{-1}, corresponding to g = 2.045(2), $|D|$ = 4.11(9) K = 2.85(6) cm^{-1}, and $N\alpha$ = 2.37(5) × 10-3 emu·mol^{-1} (solid line in Figure 9); (2) C = 4.574(4) emu·K·mol^{-1}, corresponding to g = 2.065(2), Θ = −0.68(1) K = 0.47(1) cm^{-1}, and $N\alpha$ = 2.03(4) × 10^{-3} emu·mol^{-1} (dashed line in Figure 9). Note that, as in salt **1**, it is very difficult to determine which of the two models agree better with the experimental data since, most probably, both effects (ZFS and weak antiferromagnetic

(29) O'Connor, C. J. *Prog. Inorg. Chem.* **1982**, *29*, 203 (note that the equation for $\chi_\perp$ for $S = 5/2$ presents an error in this reference).

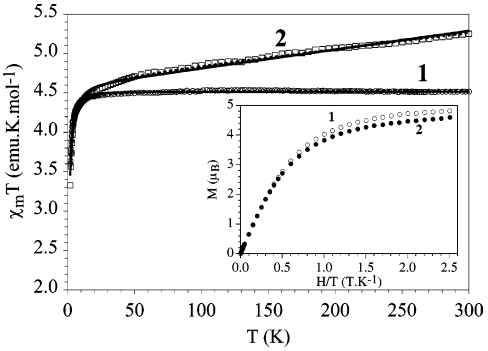

Figure 9. Thermal variation of the $\chi_m T$ product for **1** and **2**. Solid lines represent the best fit to a model of isolated $S = 5/2$ Fe(III) ions with a ZFS. Dashed lines represent the best fit to a simple Curie−Weiss law. For **2** both models include a Pauli paramagnetism. The inset shows the isothermal magnetization at 2 K for **1** and **2**.

interactions) are present in **2**. As in salt **1**, the ESR results indicate the presence in **2** of a ZFS in the Fe(III) of similar magnitude, indicating also that in compound **2** both effects, a ZFS and an a weak antiferromagnetic coupling, are present, both of similar intensities (see below). Anyway, the *C* and *N*α parameters obtained with both models are very similar and confirm the presence of Fe(III) ions with an $S = 5/2$ spin ground state with a Pauli-type paramagnetism similar to those found in many other metallic radical salts with TTF-type donors.[2] Note that, as in **1**, the sign of *D* cannot be determined from powder measurements and that the *D* value may also include the weak antiferromagnetic coupling between the Fe(III) ions. Note that in both salts the *C*, $|D|$, and Θ parameters are very similar, as expected from the similarities of both anionic layers.

Finally, we have also performed isothermal magnetization measurements at low temperature to confirm the $S = 5/2$ ground state of the $[Fe(C_5O_5)_3]^{3-}$ anion (inset in Figure 9). Both salts show very similar isothermal magnetization plots with saturation values close to 5 μ_B, as expected for high-spin Fe(III) complexes with a spin ground state of 5/2.

ESR Spectra. α-(BEDT-TTF)$_5$[Fe(C$_5$O$_5$)$_3$]·5H$_2$O (1). The room-temperature ESR spectrum of the α phase shows a central line at $g \approx 2.005$ with a line width (ΔH) of ca. 80 G that can be attributed to the BEDT-TTF donors (Figure 10a). This line is slightly anisotropic although none of the three components of the *g* factor are resolved. The anisotropy decreases when decreasing the temperature and becomes symmetric below ca. 40 K. Note that the ΔH value is slightly larger than the normal values found in α phases (40−60 G),[2] suggesting that the observed signal has also some contribution from the $S = 5/2$ Fe(III) ion in the $[Fe(C_5O_5)_3]^{3-}$ anion. This idea is supported by the thermal variation of ΔH that shows the expected smooth decrease for an α phase when decreasing the temperature to reach ca. 55 G at ca. 140 K and a smooth increase below ca. 140 K followed by a more abrupt increase below ca. 40 K (when the Fe(III) signal starts to appear) to reach a value of ca. 400 G at 4 K, indicating that the Fe(III) signal at $g \approx 2$ is also present (Figure 11). Moreover, a further support for this idea comes from the position of the BEDT-TTF signal, which does not vary with decreasing temperature from 300 to ca. 40 K and below this

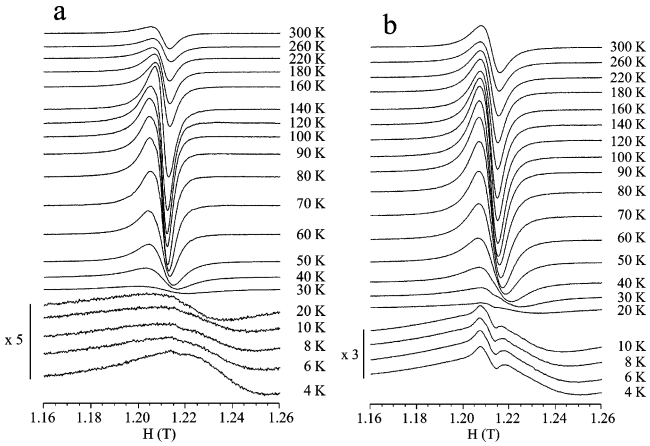

Figure 10. Q-band ESR spectra at different temperatures for the salts **1** (a) and **2** (b).

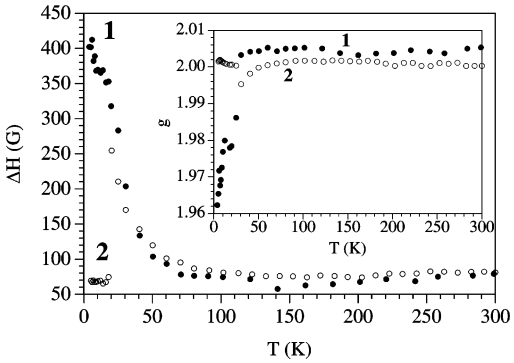

Figure 11. Thermal variation of the ESR line width (ΔH) and *g* factor (inset) for salts **1** and **2**.

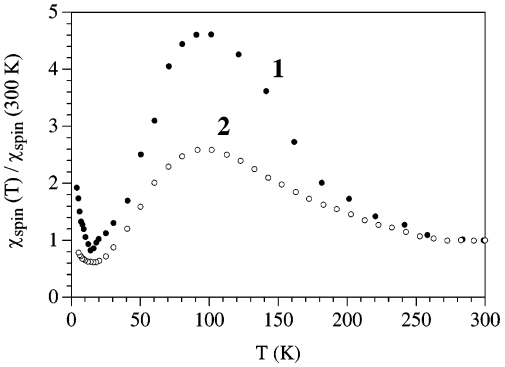

Figure 12. Thermal variation of the spin susceptibility of the BEDT-TTF layer from ESR spectra for salts **1** and **2**.

temperature shows an abrupt shift toward higher fields (lower *g* values) as a result of the overlap with the Fe(III) signal which appears only at low temperature since at high temperatures the signal broadening due to the fast spin relaxation of the Fe(III) ion precludes its observation (inset in Figure 11).

The intensity of the BEDT-TTF signal shows an increase when lowering the temperature down to ca. 100 K, where it shows a rounded maximum followed by a decrease at lower temperatures (Figure 12). This behavior suggests the presence of a strong antiferromagnetic interaction in the organic sublattice, although this contribution is small and, unfortunately, cannot be clearly separated in the SQUID magnetic susceptibility measurements since it is eclipsed by the Fe-

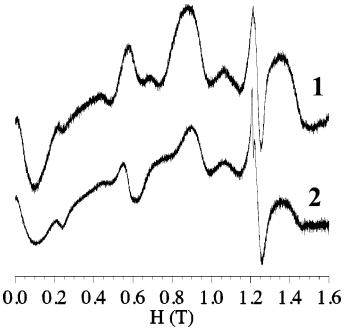

Figure 13. Q-band ESR spectra of salts **1** and **2** at 4.2 K showing the five signals arising from the $S = 5/2$ Fe(III) ion with a zero field splitting.

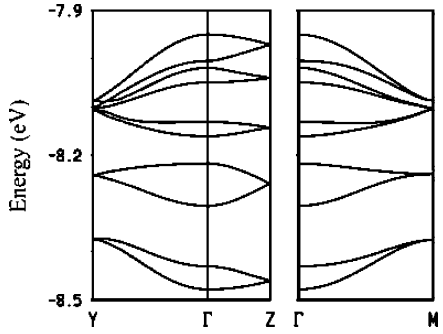

Figure 14. Calculated band structure for a donor layer of α-(BEDT-TTF)$_5$[Fe(C$_5$O$_5$)$_3$]·5H$_2$O (**1**): Γ = (0, 0); Y = (b*/2, 0); Z = (0, c*/2); M = (b*/2, c*/2).

(III) magnetic contribution. At very low temperatures the central signal of the $[Fe(C_5O_5)_3]^{3-}$ anion (at $g \approx 2$) appears split into 5 main features arising from the ZFS present in the Fe(III) ion (Figure 13), as also observed in the SQUID magnetic measurements (see above). The ESR spectrum of compound **1** at 4.2 K can be simulated with $g = 2.00$ and ZFS parameters of $|D| = 0.94$ cm^{-1} and $E = 0.010$ cm^{-1} and anisotropic Lorentzian line widths of 600 G (in the x direction) and 2000 G (in the y and z directions).

β-(BEDT-TTF)$_5$[Fe(C$_5$O$_5$)$_3$]·C$_6$H$_5$CN (2). The Q-band room-temperature ESR spectra of the β phase (**2**) is very similar to that of the α phase (**1**): it also shows a central line at $g \approx 2.001$ with a line width (ΔH) of ca. 80 G that can be attributed to the BEDT-TTF donors (Figure 10b). Note that ΔH is larger than expected for a β phase (20−30 G),[2] suggesting, as in **1**, that the observed signal has some contribution from the $S = 5/2$ Fe(III) ion in the $[Fe(C_5O_5)_3]^{3-}$ anion. This assumption is also supported by the thermal variation of ΔH that shows a thermal behavior similar to that of salt **1**: a smooth decrease with lowering the temperature, as expected for BEDT-TTF in a β phase, down to ca. 140 K (where ΔH is ca. 70 G), followed by a rapid increase below this temperature, reaching a value of ca. 250 G at 20 K, due to the presence of a large signal coming from the $[Fe(C_5O_5)_3]^{3-}$ anion (Figure 11). As in salt **1**, the g factor of the BEDT-TTF signal is also temperature independent in the 300−40 K range and shifts toward lower values (higher fields) below ca. 40 K as a result of the increase of the Fe(III) signal. Fortunately, in salt **2**, below ca. 20 K, both signals appear separated, allowing a detailed study of the BEDT-TTF signal alone in the temperature range 20−4 K (Figures 10b and 11). This study shows that ΔH is ca. 70 G for the BEDT-TTF feature at low temperatures and that the g factor is similar to that found at high temperatures (inset in Figure 11). Even more interesting is the possibility to study the spin susceptibility of the BEDT-TTF signal at low temperatures: thus the area of this signal is almost temperature independent from 20 to ca. 10 K and behaves in a paramagnetic way from 10 to 4 K. These observations are in agreement with the metallic behavior observed in the conductivity measurements between ca. 20 and ca. 10 K and with the semiconducting behavior observed below ca. 10 K. Above 20 K, the intensity of the ESR signal shows, as in salt **1**, a maximum at ca. 120 K followed by a decrease at lower temperatures (Figure 12). This behavior is very similar to that observed in the BEDT-TTF salt with the paramagnetic anion $[Fe(ox)_3]^{3-}$ and PhBr as solvent[10] and suggests the presence of a progressive charge localization, accompanied by an antiferromagnetic coupling of the BEDT-TTF molecules, starting around 120 K, in agreement with the electrical conductivity measurements (see above). Note, however, that, as observed in salt **1**, in **2** it is not possible to separate the contributions from both sublattices and, therefore, it is not possible to establish the contribution of the organic sublattice to the total magnetic moment of **2**. As in **1**, in **2** it is also possible to observe at low temperatures five main signals arising from the Fe(III) ion with ZFS (Figure 13). The simulation of the ESR spectrum of compound **2** at 4.2 K gives, as expected, the same parameters as those obtained in **1** (see above), confirming the similarities in the electronic structures of both anions in the two salts.

Band Structure Calculations. To gain some insight into the relationship between the crystal structure and transport properties of salts **1** and **2** we have carried out tight-binding band structure calculations for their donor layers. The calculated band structure near the Fermi level for **1** is shown in Figure 14. There are five pairs of bands mainly based on the ET HOMO, which pair up at the end points of the Γ → Y, Γ → Z, and Γ → M directions because of the existence of nonsymmorphic symmetry elements parallel to the b- and c-directions. Because of the stoichiometry, there are six holes to be housed in these bands. Since there is no energy gap separating the three upper bands from the others (and because of the symmetry imposed double degeneracy at Y, Z, and M, there cannot be a separation), a one-electron description of the electronic structure would predict a metallic state for this salt. However, we note that the HOMO energies of the three different donors are quite different. Whereas that for ET1 is −8.59 eV, those for ET2 and ET3 are −8.37 and −8.36 eV, respectively. The large energy difference points toward a very different charge for ET1 and ET2/ET3. This is confirmed by the analysis of the character of the different bands of Figure 14. The two lower pairs of filled bands are mainly built from the HOMO of the ET1 donor whereas the three upper pairs of bands are made of the ET2 and ET3 HOMO. This means that the ET1 donors are formally neutral. The strongly mixed ET2−ET3 character of the three upper bands means that as far as the HOMO···HOMO interactions are concerned, the ET2 and ET3 donors really form trimeric

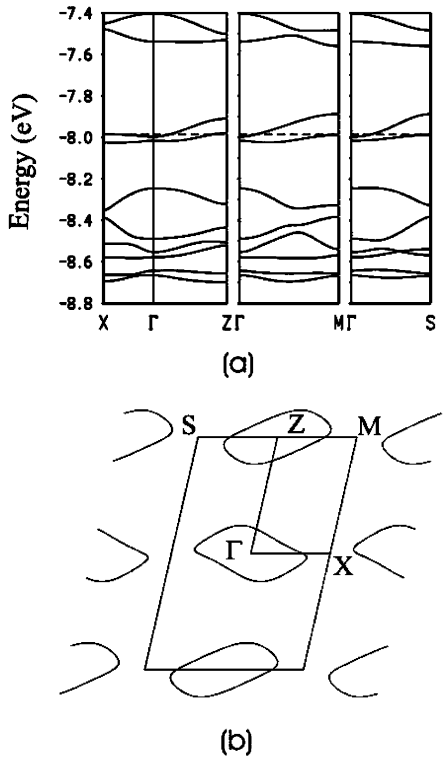

Figure 15. Calculated (a) band structure and (b) Fermi surface for a donor layer of β-(BEDT-TTF)$_5$[Fe(C$_5$O$_5$)$_3$]·C$_6$H$_5$CN (**2**). The dashed line in (a) refers to the Fermi level and Γ = (0, 0); X = (a*/2, 0); Z = (0, c*/2); M = (a*/2, c*/2); S = (−a*/2, c*/2).

units. Thus, the donor lattice of salt **1** can be described as a series of trimeric (ET2−ET3−ET2)$^{3+}$ units and neutral ET1 donors. This is consistent with the bond length analysis. As judged from the band dispersions of the three upper pairs of bands (strictly speaking the band structure is not really meaningful for a localized system but still provides a useful measure of the strength of the interactions), the direct interaction between these trimeric units is not negligible but definitely not strong. Thus, it is not surprising that the system may adopt a localized description and activated, even if relatively high, conductivity. Let us note that the Fermi surface calculated assuming a metallic filling of the bands is typical of a pseudo-one-dimensional conductor along the *b*-direction, i.e., along a direction orthogonal to the stacks direction, which is also the direction along which the Fermi surface of the α-type metallic phases like α-(ET)$_2$MHg(XCN)$_4$ (M = Tl, K Rb, NH$_4$; X = S, Se) exhibits one-dimensional components.[30]

The calculated band structure near the Fermi level for **2** is shown in Figure 15a. There are 10 bands mainly built from the donors HOMO because the repeat unit of the layer contains 10 donor molecules. The bands occur in three different groups. First, there are a pair of bands high lying in energy and neatly separated from the others. These bands are mainly based (i.e., more than 90%) on the ET1 and ET2 donors. These bands are well separated from the others because the ET1−ET2 dimerization is quite strong. Second, there are another pair of bands which are separated from both the upper and lower sets. These bands are considerably (but not exclusively) based on the ET4 donors. Typically, these bands are approximately two-thirds based on the ET4 HOMO and one-third on the ET1, ET3, and ET5 HOMOs. Third, there are a bunch of six bands, four of which have predominant ET3 and ET5 HOMO character and two of which are mainly ET1 and ET2 based. Because of the stoichiometry, there must be six holes in the bands of Figure 15a. Consequently, the upper pair of ET1 and ET2 HOMO based bands are empty whereas the next pair of bands is half-filled. These results confirm that donors ET1 and ET2 are approximately positively charged, donors ET3 and ET5 are slightly charged but not far from neutral, and ET4 should be somewhere in between ET$^{2/3+}$ and ET$^+$, in good agreement with the bond length analysis. Thus, although from the point of view of its general architecture salt **2** is a β-type phase, from the electronic perspective it is really a quite peculiar one.

The two bands of the second group overlap, and consequently, both are partially filled. This leads to the Fermi surface of Figure 15b, which contains closed electron (around Γ) and hole (around Z) pockets. The area of these holes is 10.1% of the cross section of the Brillouin zone. An important observation concerning these partially filled bands is that they are only weakly dispersive. This feature clearly points out toward a borderline electronic situation between the localized and delocalized regimes and provides a rationale for the above-mentioned conductivity results. The structural reason for the narrowness of the bands and, ultimately, for the conductivity behavior is easy to understand on the basis of the band character analysis. As mentioned, these bands are mostly ET4 in character but the different ET4 donors do not see each other directly. The fact that two of the donors (ET1 and ET2) are strongly dimerized and the remaining two (ET3 and ET5) are almost neutral is at the origin of the only moderate interaction of ET4 donors through the four other donors.

Conclusions

We have prepared the first radical salts containing the chiral [Fe(C$_5$O$_5$)$_3$]$^{3-}$ anion. Salt α-(BEDT-TTF)$_5$[Fe(C$_5$O$_5$)$_3$]·5H$_2$O (**1**) represents the first example of chirality-induced α phase and the only known pentamerized (θ_{51}) phase. Salt β-(BEDT-TTF)$_5$[Fe(C$_5$O$_5$)$_3$]·C$_6$H$_5$CN (**2**) is one of the very few examples of paramagnetic molecular metals and the only known example out of the [M(C$_2$O$_4$)$_3$]$^{3-}$ and [MX$_4$]$^{n-}$ series.[1] Furthermore, these two salts open now the possibility to study other modifications as (i) the use of other [M(C$_5$O$_5$)$_3$]$^{n-}$ complexes (M = Cr, Mn, Co, ...), (ii) the use of enantiomeric pure forms of the chiral anions to induce novel (chiral?) packings in the organic layers leading to different electrical behaviors, (iii) the change of one or more oxygen atoms by sulfur atoms in the croconate ligand, and (iv) the use of divalent paramagnetic metal atoms to induce the formation

(30) (a) Mori, H.; Tanaka, S.; Oshima, M.; Saito, G.; Mori, T.; Maruyama, Y.; Inokuchi, H. *Bull. Chem. Soc. Jpn.* **1990**, *63*, 2183. (b) Ducasse, L.; Fritsch, A. Solid State. Comm. **1994**, *91*, 201. (c) Rousseau, R.; Doublet, M. L.; Canadell, E.; Shibaeva, R. P.; Khasanov, S. S.; Rozenberg, L. P.; Kushch, N. D.; Yagubskii, E. B. *J. Phys. (Paris)* **1996**, *6*, 1527.

of extended anionic lattices as the ferro-, ferri-, and canted ferromagnetic honeycomb layers formed in the oxalate family.

Acknowledgment. This work has been supported by the Spanish MEC (Project MAT2004-03849), the DGI-Spain (Project FIS2006-12117-C04-01), the Generalitat de Catalunya (Project 2005 SGR 683), the European Union (MAGMANet network of excellence. Project SwMaCo on Multifunctional molecuar materials COST Action D35-0011-05 on "Multifunctional and switchable molecular materials"), and MIUR (PRIN 2005033828 project). C.G.-S. thanks the MEC for a research contract (Programa Ramón y Cajal).

Supporting Information Available: Interplanar distances (Å) and angles (deg) of the BEDT-TTF molecules in the organic layers in **1** and **2** (Table S1) and CIF files of the two structures. This material is available free of charge via the Internet at http://pubs.acs.org.

IC062152M